Phytomedicine 134 (2024) 155959

Contents lists available at ScienceDirect

Phytomedicine

journal homepage: www.elsevier.com/locate/phymed

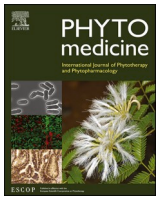

Original Article

β,β-Dimethylacrylalkannin, a key component of Zicao, induces cell cycle arrest and necrosis in hepatocellular carcinoma cells

Li-Sha Shen [a,b], Jia-Wen Chen [c,d], Rui-Hong Gong [e], Zesi Lin [f], Yu-Shan Lin [c], Xing-Fang Qiao [a,b], Qian-Mei Hu [a,b], Yong Yang [a,b,*], Sibao Chen [c,d,e,g,**], Guo-Qing Chen [c,e,g,*]

[a] Chongqing Academy of Chinese Materia Medica, Chongqing 400065, PR China
[b] Sichuan-Chongqing Joint Key Laboratory of Innovation of New Drugs of Traditional Chinese Medicine, Chongqing 400065, PR China
[c] State Key Laboratory of Chinese Medicine and Molecular Pharmacology (Incubation), The Hong Kong Polytechnic University Shenzhen Research Institute, Shenzhen 518057, PR China
[d] Institute of Medicinal Plant Development, Chinese Academy of Medical Sciences and Peking Union Medical College, Beijing 100193, PR China
[e] Department of Food Science and Nutrition, The Hong Kong Polytechnic University, Hung Hom, Hong Kong S.A.R., PR China
[f] Southern Medical University Hospital of Integrated Traditional Chinese Medicine and Western Medicine, Southern Medical University, Guangzhou 510315, PR China
[g] Research Centre for Chinese Medicine Innovation, The Hong Kong Polytechnic University, Hung Hom, Hong Kong S.A.R., PR China

ARTICLE INFO

Keywords:
β,β-Dimethylacrylalkannin
Zicao
Traditional Chinese medicine
Hepatocellular carcinoma
Cell cycle
Necrosis

ABSTRACT

Background: β,β-Dimethylacrylalkannin (DMAKN), a natural naphthoquinone found in Zicao, a traditional Chinese medicine (TCM), serves as the designated quantitative marker in the Chinese Pharmacopoeia. Despite its established role in assessing Zicao quality, DMAKN's biological potential remains underexplored in research.
Methods: We investigated DMAKN's involvement in Zicao's anti-hepatocellular carcinoma (HCC) properties using a combination of HPLC content analysis and comprehensive bioinformatics. Subsequently, both *in vitro* and *in vivo* experiments were conducted to evaluate DMAKN's efficacy against HCC. Mechanistic investigations focused on elucidating DMAKN's impact on cell cycle regulation and induction of cell death.
Results: Integrated HPLC analysis and bioinformatics identified DMAKN as the primary active compound responsible for Zicao's anti-HCC activity. *In vitro* and *in vivo* studies confirmed DMAKN's potent efficacy against HCC. Notably, DMAKN demonstrated dual effects on HCC cells: inhibiting proliferation at lower doses and inducing rapid cell death at higher doses. Mechanistic insights revealed that low-dose DMAKN induced G2/M phase cell cycle arrest through modulation of CDK1 and Cdc25C phosphorylation, while high-dose DMAKN triggered necrosis. Importantly, high-dose DMAKN caused a sharp increase in intracellular ROS levels in a short time, while low-dose DMAKN gradually increased ROS levels over a long period. Additionally, low-dose DMAKN-induced ROS activated the JNK pathway, crucial for cell cycle arrest, whereas high-dose DMAKN-induced necrosis was ROS-dependent but JNK-independent.
Conclusion: This study underscores DMAKN's pivotal role as the principal anti-HCC compound in Zicao, delineating its differential effects and underlying mechanisms. These results demonstrate the potential of DMAKN as a therapeutic agent for the treatment of HCC, providing important information for further study and advancement in cancer therapy.

Abbreviations: DMAKN, β,β-dimethylacrylalkannin; TCM, traditional Chinese medicine; HCC, hepatocellular carcinoma; HPLC, high-performance liquid chromatography; ROS, reactive oxygen species; CDK1, cyclin-dependent kinase 1; Cdc25C, cell division cycle 25C; NAC, n-acetyl cysteine; STS, staurosporine; Fer-1, ferrostatin-1; Nec-1, necrostatin-1; MTT, 3-[4,5-dimethylthiazol-2-yl]-2,5 diphenyl tetrazolium bromide; PI, propidium iodide; FITC, fluorescein isothiocyanate; DEGs, differentially expressed genes; JNK, Jun N-terminal kinase; ATCC, american type culture collection; DMEM, dulbecco's nodified eagle nedium; ECL, chemiluminescence; FBS, fetal bovine serum; TCGA, the cancer genome atlas; PPI, protein-protein interaction; 3D, three-dimensional; DCFH-DA, 2′,7′-dichlorodihydrofluorescein diacetate; co-IP, co-immunoprecipitation.

* Corresponding author: Chongqing Academy of Chinese Materia Medica. No. 34, Nanshan Road, Nan'an District, Chongqing 400065, PR China.
** Corresponding author: State Key Laboratory of Chinese Medicine and Molecular Pharmacology (Incubation), The Hong Kong Polytechnic University Shenzhen Research Institute. No. 18, Yuexing 1st Road, Nanshan District, Shenzhen 518057, PR China.
E-mail addresses: yangychem@cqacmm.com (Y. Yang), sibao.chen@polyu.edu.hk (S. Chen), guoqing.chen@polyu.edu.hk (G.-Q. Chen).

https://doi.org/10.1016/j.phymed.2024.155959
Received 12 May 2024; Received in revised form 2 August 2024; Accepted 14 August 2024
Available online 19 August 2024

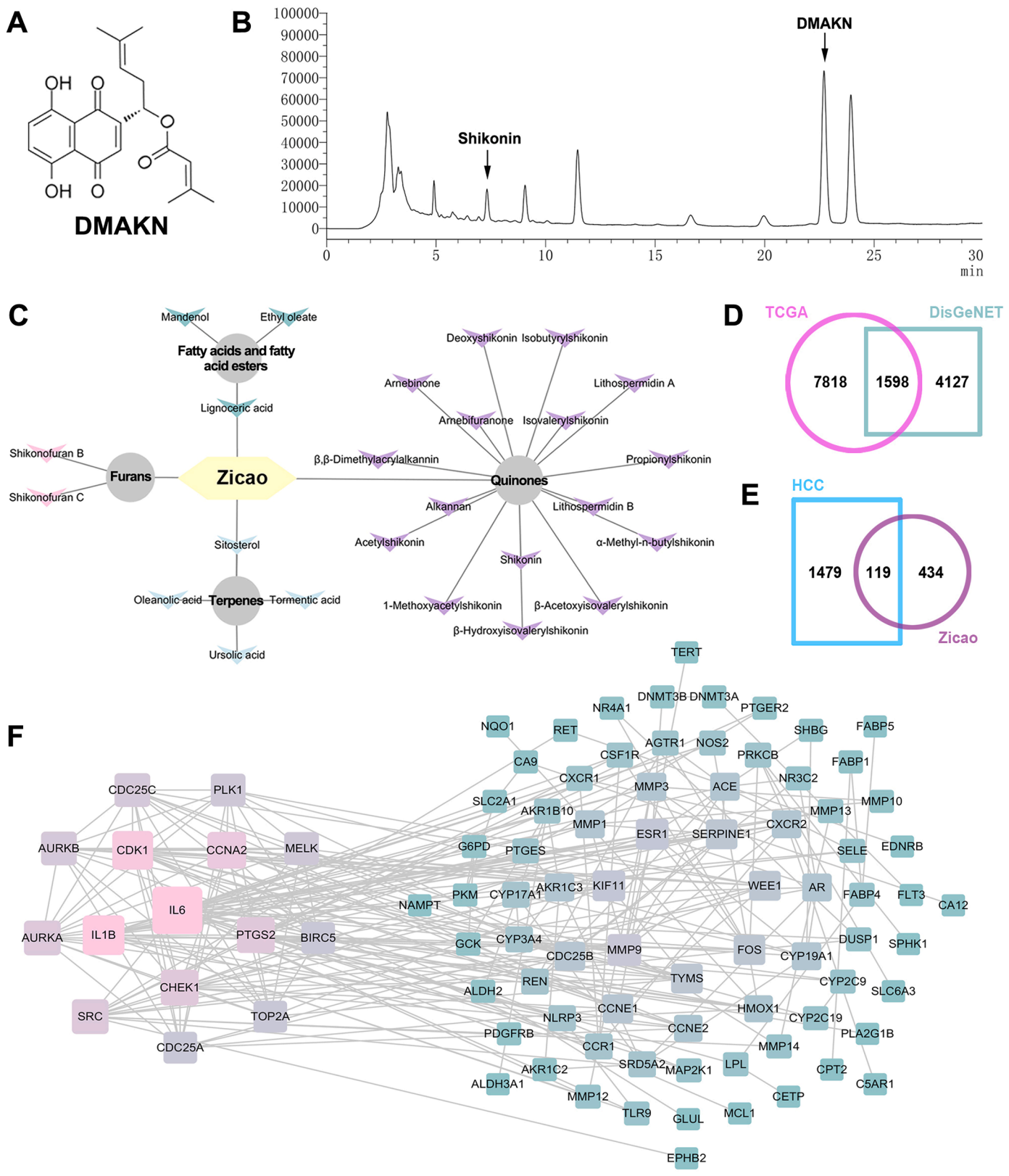

Fig. 1. DMAKN was identified as the crucial active ingredient responsible for the anti-HCC effects in Zicao. (A) Chemical structure of DMAKN. (B) HPLC method used for analyzing the content of shikonin and DMAKN in Zicao herbs. (C) Visualization of a total of 25 active ingredients in Zicao, along with their structural types. (D) Overlapped HCC-related targets between TCGA and DisGeNET database. (E) Overlapped targets between HCC-related targets and Zicao-related targets. (F) Visualization of a PPI network for potential targets of Zicao.

Introduction

Liver cancer is the sixth most diagnosed cancer and the third leading cause of cancer-related deaths, represents a significant global health challenge (Sleeman et al., 2019). Hepatocellular carcinoma (HCC) is the predominant type of primary liver cancer, accounting for 75 %–85 % of all cases (Sung et al., 2021). Despite the availability of surgical options, many patients diagnosed at late stages of HCC resort to systemic therapies, which are primarily medications that circulate throughout the body to target cancer cells. These therapies are crucial as initial interventions and substantially impact patient outcomes (Fan et al., 2022). Systemic therapies for HCC encompass multi-targeted tyrosine kinase inhibitors (TKIs) such as sorafenib and lenvatinib (Mou et al., 2021). These TKIs target multiple pathways crucial for HCC growth and angiogenesis. Another notable advancement is the combination of atezolizumab, a PD-L1 monoclonal antibody, and bevacizumab, an anti-VEGF antibody (de Castro et al., 2022). This dual therapy harnesses complementary mechanisms of immune checkpoint inhibition and anti-angiogenic action, thereby enhancing the body's immune response against HCC cells while depriving them of essential nutrients. Furthermore, the combination of durvalumab, a PD-L1 inhibitor, with tremelimumab, a CTLA-4 inhibitor, offers a dual immune checkpoint blockade (Abou-Alfa et al., 2022). This strategy aims to maximize the immune system's ability to recognize and destroy HCC cells by blocking two distinct immune checkpoint pathways. While these first-line systemic therapies show survival benefits, they are not without significant challenges. Patients often develop resistance, face considerable side effects, and experience financial burdens. Therefore, there is a pressing need for innovative HCC therapies that can overcome these challenges and improve patient outcomes.

Natural products have played a foundational role in drug discovery, particularly in cancer research advancement (Chunarkar-Patil et al., 2024). Compounds like paclitaxel, vincristine, and camptothecin, derived from natural sources, have been widely applied in cancer therapy. Traditional Chinese medicine (TCM) is a rich source of natural products with therapeutic potential (Li et al., 2022). In recent decades, the isolation and identification of bioactive natural products from TCM have emerged as central focuses in modern TCM research (Yuan et al., 2016).

Zicao, the root of *Lithospermum erythrorhizon* Sieb. et Zucc, *Arnebia euchroma* (Royle) Johnst, or *Arnebia guttata* Bunge, is a TCM herb celebrated for its anti-inflammatory and anticancer properties, particularly against HCC(Yan et al., 2017). Shikonin, a prominent and extensively studied component of Zicao, is renowned for its anticancer properties (Guo et al., 2019). Interestingly, the Chinese Pharmacopoeia uses DMAKN (Fig. 1A), rather than shikonin, as the quantitative marker for Zicao quality control (Sha et al., 2024). Despite its importance, DMAKN is less explored for its biological effects. This study aims to uncover the role of DMAKN as a key ingredient responsible for the activity of Zicao, and to explore its specific anticancer effects on HCC, with the goal of elucidating the potential mechanism of this compound.

Materials and methods

Reagents

Chemicals, including DMAKN, shikonin, PI, NAC, Fer-1, Nec-1, SP600125, and z-VAD-fmk were sourced from MedChemExpress (Shanghai, China). The primary antibodies used were as follows: p-CDK1 (Thr14) (Beyotime, AF5758), p-CDK1 (Thr161) (Beyotime, AF5764), p-CDK1 (Tyr15) (Beyotime, AF5761), Cyclin B1 (Beyotime, AF6627), Cdc25C (Beyotime, AF6462), p-Cdc25c (Immunoway, YP0058), CDK1 (Beyotime, AF0111), caspase-3 (CST, 9662), PARP (CST, 9542), GPX4 (Beyotime, AF7020), SLC7A11 (Beyotime, AF7992), MLKL (Beyotime, AF5231), RIP1 (Beyotime, AF7896), and GAPDH (Santa Cruz, 365,062). HRP-goat anti-mouse and HRP-goat anti-rabbit secondary antibodies (Invitrogen, 32,460) were used in our study.

Bioinformation analysis

The ingredients in Zicao were collected from TCMSP (http://tcmspw.com/tcmsp.php). SwissTargetPrediction (http://www.swisstargetprediction.ch/) was utilized to predict molecular targets. Data of HCC-related genes were sourced from DisGeNET (https://www.disgenet.org/), and gene expression profiles were extracted from TCGA (https://portal.gdc.cancer.gov/). HCC-related gene expression data from TCGA were analyzed using the R package "DESeq2″ to identify DEGs with $|log2FC| > 1$ and $p < 0.05$. HCC-related DEGs were found to overlap with Zicao targets. To further analyze PPI, we employed the STRING online platform (https://string-db.org/), utilizing a confidence score threshold > 0.4.

Cell culture

HepG2 and Huh7 cell lines were provided from ATCC. They were cultured in DMEM, supplemented with 10 % FBS, under conditions of 37 °C and 5 % CO_2. For 3D cell culture, 96-well plates were coated with 2 % agarose in serum-free DMEM. After seeding 1×10^3 cells per well, spheroids were treated with DMAKN and observed daily under a microscope.

MTT assay for comparing the anti-HCC efficacy between shikonin and DMAKN

Cells were seeded at 5×10^3 cells/well in 96-well plates. They were separately treated with shikonin and DMAKN at various doses and time points to evaluate their inhibitory effects on HCC cell viability. Cell viability was then assessed to compare the anti-HCC efficacy of shikonin and DMAKN *in vitro*.

Xenograft tumor model for evaluating the in vivo anti-HCC efficacy of DMAKN

Male BALB/c nude mice were provided from ZhuHai Bestest Biotechnology Co., Ltd. Huh7 cells, at a density of 5×10^6 in 0.1 ml DMEM, were subcutaneously injected into the right flank of each mouse. Upon reaching a tumor volume of approximately 100 mm^3, the mice were randomly assigned to three groups ($n = 4$): (i) the Vehicle group, administered oral saline; (ii) the DMAKN-low group, administered DMAKN (5 mg kg^{-1}) *via* oral gavage; and (iii) the DMAKN-high group, administered DMAKN (20 mg kg^{-1}) *via* oral gavage. Tumor dimensions were measured daily to calculate tumor volumes. After a 14-day treatment period, the mice were humanely euthanized using CO_2 inhalation. Subsequently, the tumors were excised, weighed, and preserved for further analysis.

Cell death quantification

Cells were plated in 6-well plates at a density of 5×10^5 cells/well, 24 h prior to DMAKN treatment. Following treatment, PI was incorporated into the culture media to facilitate flow cytometry analysis and quantify PI-positive cells.

Cell cycle assay

Cells were seeded in 6-well plates at 5×10^5 cells/well 24 h before DMAKN treatment. After 24 h of DMAKN treatment, cells were fixed, stained with PI and RNase, and analyzed for cell cycle phases using flow cytometry.

Apoptosis assay

Cells were plated in 6-well plates at 5×10^5 cells/well 24 h before DMAKN treatment. After 4 h of DMAKN treatment, flow cytometry with Annexin V/PI double staining was conducted following the kit instructions (Beyotime Biotechnology, C1062L).

Western blotting analysis

Proteins were extracted from HCC cells using RIPA lysis buffer, followed by centrifugation. Equal quantities of protein were separated *via* SDS-PAGE and then transferred onto PVDF membranes. After blocking, the membranes were incubated with primary antibodies at 4 °C overnight. The following day, the membranes were further incubated with secondary antibodies for 1 h. The immune-reactive proteins were then detected using enhanced ECL.

ROS measurement

Cells were seeded in 6-well plates at 5×10^5 cells/well 24 h prior to DMAKN treatment. After that, cells were incubated for 1 h with 20 μM DCFH-DA. Then ROS generation was analyzed using flow cytometry.

Transfection of siRNA

GenePharma (Shanghai, China) provided the siRNA sequences targeting JNK. The specific sequences used were 5′-AAAGAAUGUCCUACCUUCUUU-3′ and 5′-AGAAGGUAGGACAUUCUUU-3′. Opti-MEM medium and Lipofectamine 3000 reagent were used for transfection, following the manufacturer's instructions. The efficiency of JNK knockdown was assessed *via* western blotting 72 h post-transfection.

Statistical analysis

Data are expressed as mean ± standard error from three independent experiments. Statistical significance was assessed using one-way analysis of variance (ANOVA) with GraphPad Prism 8.0 software. Results were considered statistically significant when $p < 0.05$.

Results

DMAKN as the crucial active ingredient is responsible for the anti-HCC effects in Zicao

Our investigation began by analyzing shikonin and DMAKN contents in Zicao herbs using HPLC. Our results, depicted in Fig. 1B, show significantly higher DMAKN levels, surpassing shikonin, which is consistent with previous studies(SHI et al., 2018). This underscores DMAKN's role as the quantitative marker for Zicao quality in the Chinese Pharmacopoeia(Sha et al., 2024).

Concurrently, bioinformatics analysis was conducted to assess the potential anti-HCC activity of Zicao ingredients. Using the TCMSP database, we identified 51 Zicao-associated ingredients and filtered them based on $DL > 0.15$, resulting in 39 compounds. After excluding ingredients lacking structure and target information, a total of 25 active compounds were screened from PubChem as Zicao's active ingredients. These compounds, primarily quinones, constitute the principal active constituents (64 %) of this herb, accompanied by terpenes, furans, fatty acids, and fatty acid esters (Fig. 1C). Subsequently, we predicted the molecular targets of these 25 compounds using SwissTargetPrediction, resulting in 533 potential targets of Zicao (**Tab. S1**). Additionally, we gathered 9416 DEGs related to HCC from TCGA and 5725 therapeutic targets for HCC from DisGeNET. Among these, 1598 targets overlapped with HCC targets, as shown in Fig. 1D and **Tab. S2**. Further analysis revealed 119 targets that may serve as differentially expressed anti-HCC targets for Zicao, as depicted in Fig. 1E and **Tab. S3**.

Table 1
The proportion of hub targets regulated by compounds.

No.	Compound	Ratio	Target
1	β,β-Dimethylacrylalkannin	5/15	CHEK1,PTGS2,SRC,AURKB,PLK1
2	Ursolic acid	4/15	IL6,IL1B,PTGS2,BIRC5
3	Oleanolic acid	4/15	IL6,PTGS2,TOP2A,CDC25A
4	β-Hydroxyisovalerylshikonin	4/15	CDK1,PTGS2,CHEK1
5	β-Acetoxyisovalerylshikonin	4/15	CHEK1,PTGS2,AURKB,MELK
6	Propionylshikonin	4/15	CHEK1,SRC,AURKB,PLK1
7	Isovalerylshikonin	4/15	CHEK1,PTGS2,AURKB,MELK
8	Isobutyrylshikonin	3/15	SRC,PLK1,CHEK1
9	Arnebifuranone	3/15	CDC25C,CDC25A,SRC
10	Alkannan	3/15	CDC25C,CDC25A,CDK1
11	Acetylshikonin	2/15	SRC,CDK1
12	Shikonofuran B	2/15	CDK1,AURKA
13	Lithospermidin B	2/15	CDK1,PTGS2
14	Lithospermidin A	2/15	CDK1,PTGS2
15	α-Methyl-n-butylshikonin	1/15	CDK1
16	Shikonin	1/15	PTGS2
17	Deoxyshikonin	1/15	CDC25A
18	Arnebinone	1/15	CDK1
19	1-Methoxyacetylshikonin	1/15	PTGS2
20	Shikonofuran C	1/15	PTGS2
21	Mandenol	1/15	PTGS2
22	Ethyl oleate	1/15	PTGS2
23	Tormentic acid	0/15	–
24	Sitosterol	0/15	–
25	Lignoceric acid	0/15	–

To identify potential protein targets of Zicao, a PPI network, comprising 91 nodes and 254 edges, was constructed using data from STRING (Fig. 1F). Using CytoHubba in Cytoscape, we ranked the top 15 proteins by Degree. These hub targets, crucial for Zicao therapy of HCC, have direct connections with multiple proteins. Notably, DMAKN emerged with the highest hub targets, constituting 33.3 % (5/15). In contrast, shikonin had only one hub target (Table 1). These findings suggest that DMAKN exhibits stronger efficacy in HCC compared to other compounds, including shikonin. Given the higher content of DMAKN within the Zicao herb, these findings collectively support the crucial role of DMAKN as the active ingredient responsible for the anti-HCC effects in Zicao.

DMAKN exhibits significant anti-HCC activity both in vitro and in vivo

To validate DMAKN's anticancer potential against HCC, we used shikonin as a positive control due to its well-documented anticancer activity across various cancers, including HCC (Gong and Li, 2011; Wei et al., 2013). HepG2 and Huh7, two HCC cell lines, were employed to assess the impact of DMAKN and shikonin on cell viability using MTT assay. Fig. 2A illustrates a notable reduction in cell viability in both HepG2 and Huh7 cells following DMAKN treatment. Importantly, there was no significant difference between the effects of DMAKN and shikonin, confirming that DMAKN also exhibits significant anti-HCC activity. Subsequent colony formation assays (**Fig. S1**) further affirmed DMAKN's substantial suppression of colony formation in both cell lines, underscoring its strong anti-HCC activity *in vitro*.

To evaluate the *in vivo* anti-HCC efficacy of DMAKN, we employed a xenograft mouse model and administered DMAKN at two different doses. As depicted in Fig. 2B, the vehicle group exhibited a marked increase in tumor volume over time. In contrast, tumor growth in both the DMAKN-low and DMAKN-high groups was significantly inhibited, with the high-dose group showing a more pronounced reduction in tumor volume increase. After 14 days, the mice were euthanized, and the xenograft tumors were excised for evaluation. Fig. 2C shows that tumors in both DMAKN-treated groups were smaller than those in the vehicle group, with the high-dose group demonstrating the most significant reduction in tumor size. Fig. 2D presents the tumor masses for each group, indicating that both the low-dose and high-dose groups had significantly lower tumor masses compared to the vehicle group, with

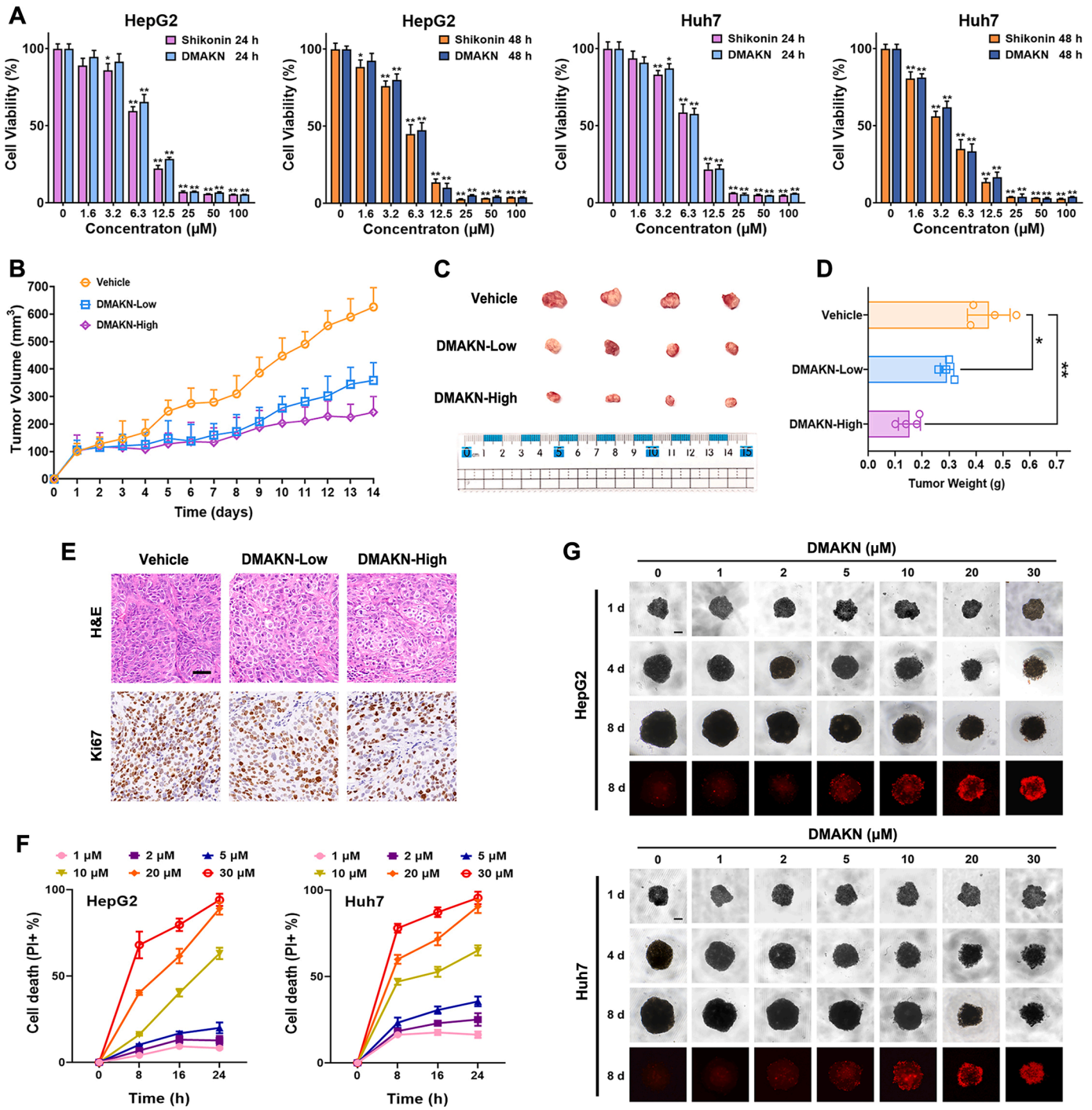

Fig. 2. DMAKN exhibited anti-HCC effects. (A) The MTT assay was used to evaluate the viabilities of HepG2 and Huh7 cells treated with DMAKN and shikonin. (B) Over the course of the experiment, measurements of the HCC tumor volumes were consistently recorded. (C) HCC tumors images were taken. (D) HCC tumor weights were noted. * $p < 0.05$, ** $p < 0.01$. (E) HCC tumors were subjected to H&E staining, followed by immunohistochemical staining for Ki67. Scale bar=50 μm. (F) Using flow cytometry, the percentage of cell death in HepG2 and Huh7 cells treated to different doses of DMAKN was determined, identifying PI-positive cells. (G) Using a 3D *in vitro* model, HepG2 and Huh7 cells were treated with different doses of DMAKN. Spheroid volumes were monitored, and images were captured. On the final day, PI staining was used to identify dead cells. Scale bar=100 μm.

the high-dose group having the smallest mass. Additionally, H&E staining revealed distinct morphological differences, with both DMAKN-treated groups exhibiting noticeable vacuole presence (Fig. 2E). Furthermore, reduced Ki67 expression in tumor tissues from both DMAKN-treated groups confirmed the compound's potent anti-HCC activity *in vivo*.

The effects of DMAKN on HCC cells vary distinctly based on its dosage

The MTT assay (Fig. 2A) revealed DMAKN's ability to inhibit HCC cell viability, underscoring its role in suppressing cell proliferation. To explore further, we assessed DMAKN's potential to induce cell death in HCC cells, a critical consideration in developing anticancer agents (Lin et al., 2024). PI staining combined with flow cytometry was utilized for this purpose, with findings detailed in Fig. 2F, **S2** and **S3**. At doses of 10

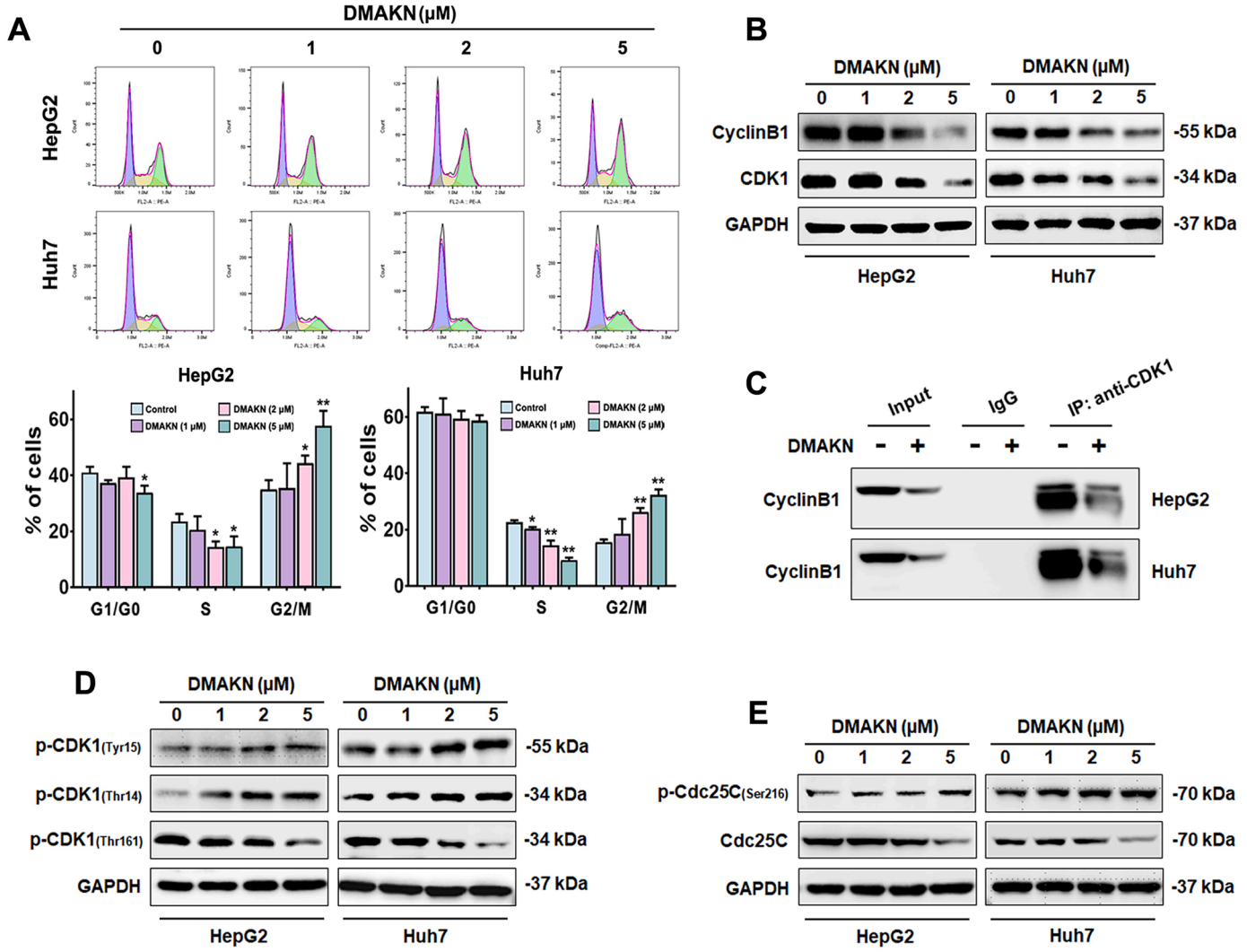

Fig. 3. Low-dose DMAKN induced G2/M cell cycle arrest and modulated CDK1 phosphorylation status. (A) Flow cytometry analyses (upper panel) illustrated the cell cycle distribution of two HCC cell lines after 24 h of low-dose DMAKN (1, 2, and 5 μM) treatment. The lower panel quantified the percentage of cells in each phase. * $p < 0.05$, ** $p < 0.01$. (B) Western blotting assays depicted the expression levels of CDK1 and Cyclin B1 in HCC cells treated with low-dose DMAKN (1, 2, and 5 μM) for 24 h. (C) Co-IP assay revealed an interaction between CDK1 and Cyclin B1 in HCC cells treated with DMAKN (5 μM) for 24 h. (D) Western blotting assays showed the modulation of CDK1 phosphorylation at Tyr-15, Thr-14, and Thr-161 in HCC cells treated with low-dose DMAKN (1, 2, and 5 μM) for 24 h. (E) Western blotting assays illustrated the regulation of Cdc25C phosphorylation at Ser-216 in HCC cells treated with low-dose DMAKN (1, 2, and 5 μM) for 24 h.

μM or higher, DMAKN rapidly induced HCC cell death within a short duration. Moreover, as exposure time increased, the incidence of HCC cell death due to high doses of DMAKN (≥ 10 μM) significantly rose, indicating a pronounced trend. Conversely, doses equal to or below 5 μM resulted in minimal cell death, with no substantial increase observed over time. These results suggest that DMAKN exerts its anti-HCC effect primarily through inhibition of proliferation at low doses, while at higher doses, it directly induces HCC cell death to achieve its anti-HCC effect.

To validate the divergent effects of DMAKN doses on HCC cells, we employed a 3D *in vitro* cell culture model, which provides a microenvironment similar to human tumors for improved drug screening (Nath and Devi, 2016). Fig. 2G depicts the outcomes of this model, showcasing suppressed spheroid growth in DMAKN-treated groups compared to untreated ones. Notably, spheroids in high-dose groups exhibited minimal growth, with sparse edges and scattered single cells. Upon PI staining, a significant portion of cells within high-dose group spheroids exhibited staining, while fewer cells within low-dose group spheroids showed staining, despite volume growth inhibition. These findings underscore that while low DMAKN doses inhibit cell spheres without inducing cell death, high doses directly trigger cell death in 3D spheroids, emphasizing the different impact of DMAKN on HCC cells.

DMAKN induces G2/M cell cycle arrest at low doses

Considering the reliance of cell proliferation on cell cycle progression(Collins et al., 1997), we examined cell cycle distribution in HCC cells treated with low doses of DMAKN. As depicted in Fig. 3A, there was a significant increase in the percentage of cells in the G2/M phase and a corresponding decrease in the S phase, indicating that DMAKN arrests the cell cycle at the G2/M phase, thereby inhibiting proliferation. Given the critical role of CDK1 and Cyclin B1 in orchestrating the transition through the G2/M phase (Gong et al., 2024), we investigated the impact of DMAKN on these proteins. Fig. 3B shows a consistent reduction in Cyclin B1 and CDK1 expression across HepG2 and Huh7 cells following low-dose DMAKN treatment. Furthermore, co-IP analysis, as shown in Fig. 3C, confirmed diminished binding between CDK1 and Cyclin B1 under low-dose DMAKN treatment. These findings underscore DMAKN's efficacy in suppressing Cyclin B1 and CDK1 expression and disrupting their interaction, ultimately leading to G2/M cell cycle arrest in HCC

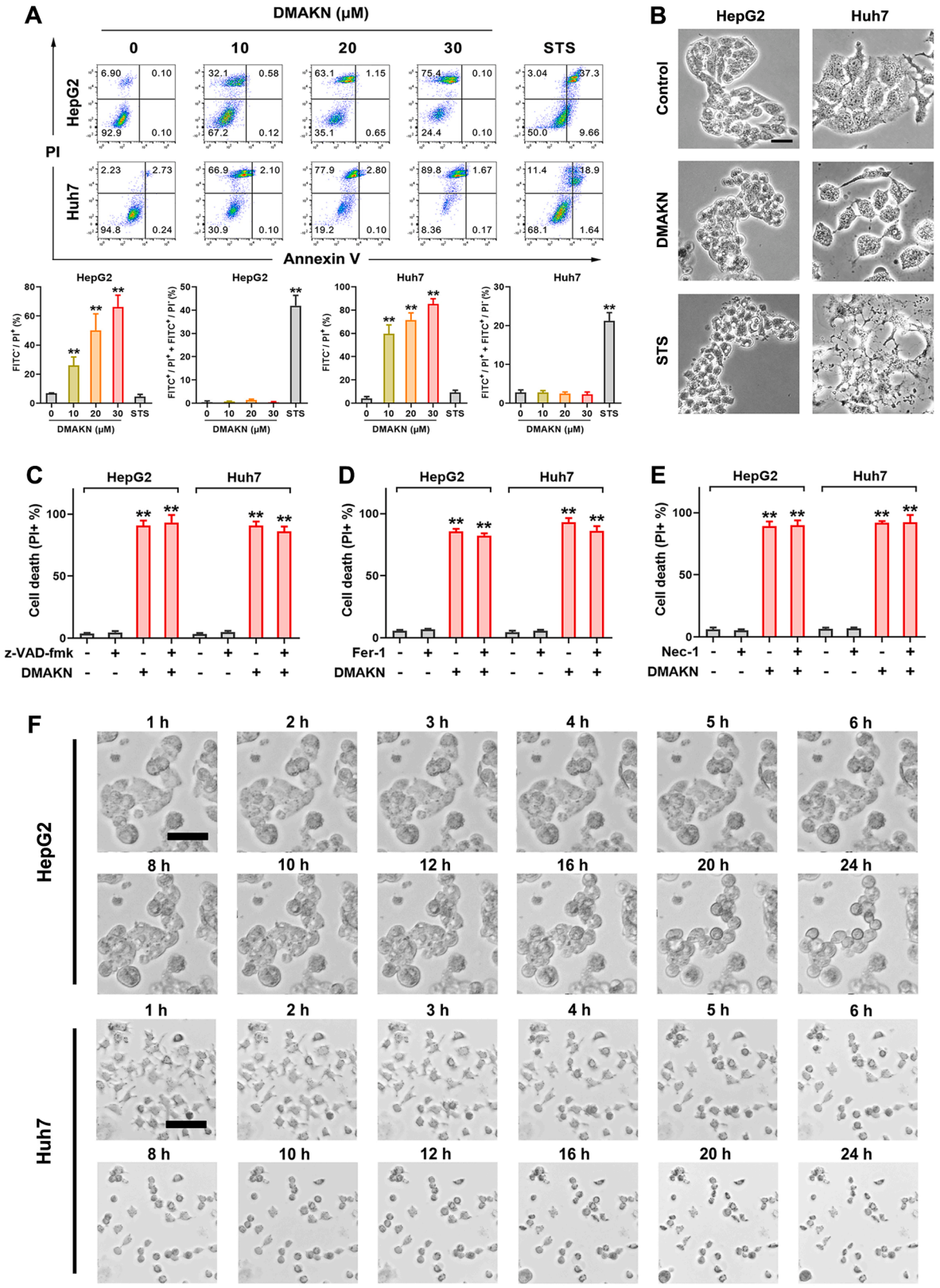

Fig. 4. High-dose DMAKN induced necrosis in HCC cells. (A) Flow cytometry analyses (upper panel) revealed distinct Annexin V-FITC/PI staining patterns between high-dose DMAKN (10, 20, and 30 μM) and 10 μM STS after 8 h of treatment. The lower panel quantifies the percentage of cells exhibiting different staining patterns between high-dose DMAKN and STS. ** $p < 0.01$. (B) Morphological changes in HCC cells exposed to DMAKN (30 μM) and STS (10 μM) for 8 h. Scale bar=10 μm. (C) Cell death in HCC cells treated with DMAKN (30 μM) alone and with the apoptotic inhibitor z-VAD-fmk (20 μM) for 24 h. ** $p < 0.01$. (D) Cell death in HCC cells treated with DMAKN (30 μM) alone and with the ferroptotic inhibitor Fer-1 (2 μM) for 24 h. ** $p < 0.01$. (E) Cell death in HCC cells treated with DMAKN (30 μM) alone and with the necroptotic inhibitor Nec-1 (10 μM) for 24 h. ** $p < 0.01$. (F) Live-cell analysis images capturing morphological changes in HCC cells treated with 30 μM DMAKN. Scale bar=50 μm.

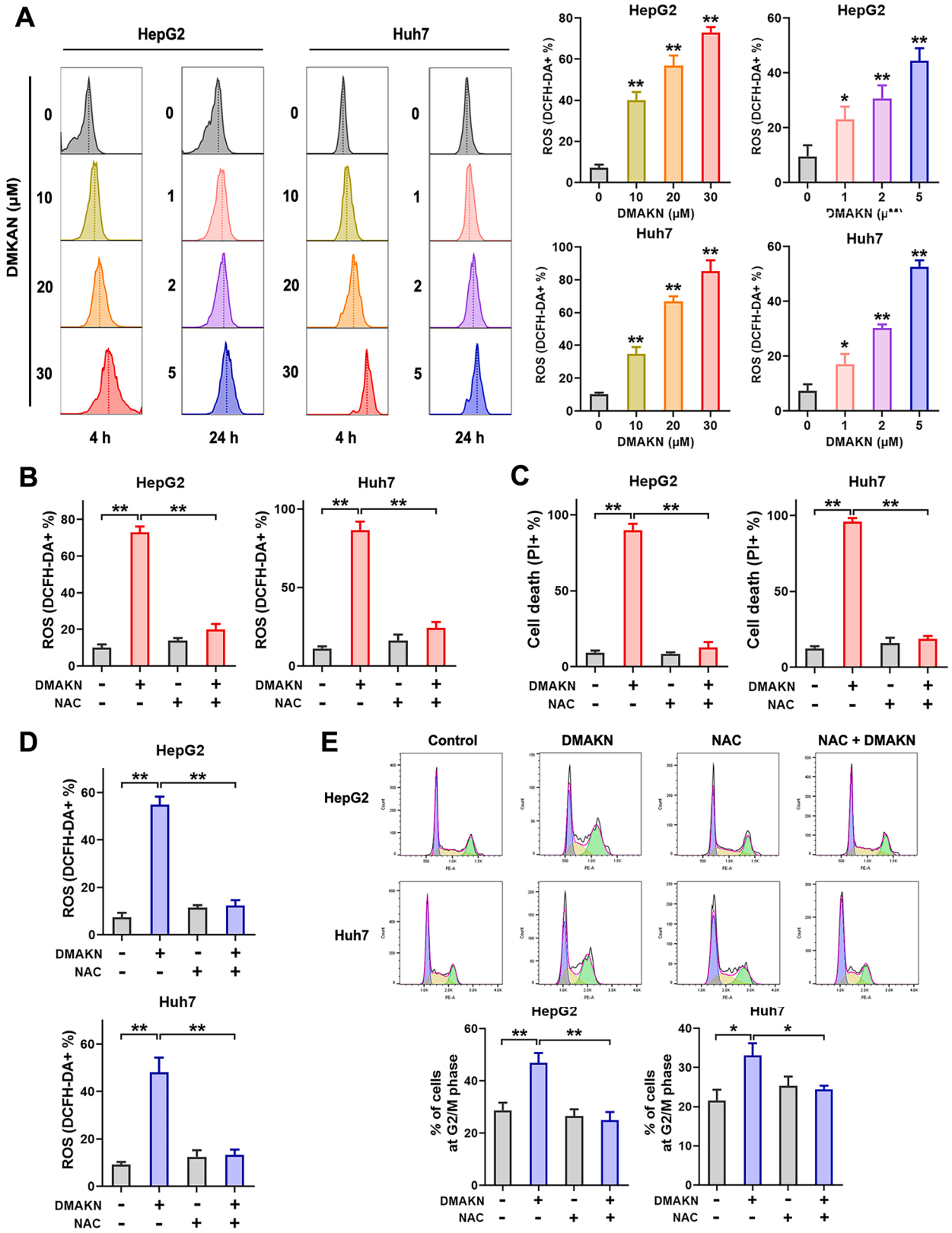

Fig. 5. Low-dose and high-dose DMAKN both increased cellular ROS levels. (A) Flow cytometry analyses (left panel) demonstrated the increased ROS levels in HCC cells treated with high-dose DMAKN (10, 20, and 30 μM) for 4 h and low-dose DMAKN (1, 2, and 5 μM) for 24 h. The right panel quantified the percentage of HCC cells staining with DCFH-DA under these dosage conditions. * $p < 0.05$, ** $p < 0.01$. (B) ROS levels in HCC cells exposed to DMAKN (30 μM) with or without NAC (2 mM) for 4 h. ** $p < 0.01$. (C) Cell death in HCC cells exposed to DMAKN (30 μM) with or without NAC (2 mM) for 24 h. ** $p < 0.01$. (D) ROS levels in HCC cells exposed to DMAKN (5 μM) with or without NAC (2 mM) for 24 h. ** $p < 0.01$. (E) Flow cytometry analyses (upper panel) illustrated the cell cycle distribution of two HCC cell lines following 24 h of treatment with DMAKN (5 μM) with or without NAC (2 mM). The lower panel quantified the percentage of cells in the G2/M phase of the cell cycle. * $p < 0.05$, ** $p < 0.01$.

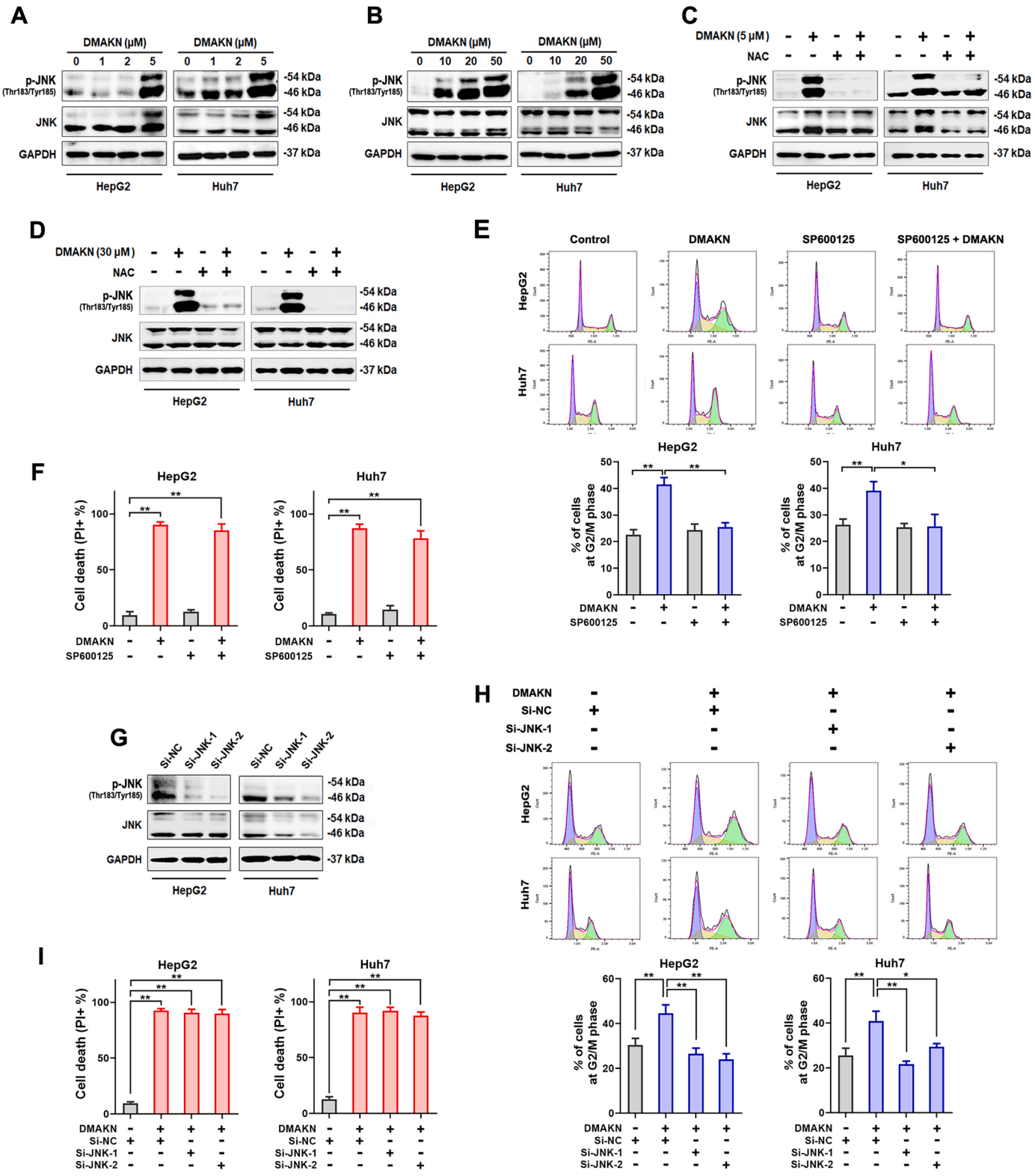

Fig. 6. DMAKN regulated JNK pathway at low and high doses. (A) Western blotting analysis showed the activation of the JNK pathway in HCC cells treated with low doses of DMAKN (1, 2, and 5 μM) for 24 h. (B) Western blotting analysis showed the activation of the JNK pathway in HCC cells treated with high doses of DMAKN (10, 20, and 30 μM) for 4 h. (C) Western blotting analysis of the JNK pathway in HCC cells exposed to DMAKN (5 μM) with or without NAC (2 mM) for 24 h. (D) Western blotting analysis of the JNK pathway in HCC cells exposed to DMAKN (30 μM) with or without NAC (2 mM) for 4 h. (E) Flow cytometry analyses (upper panel) illustrated the cell cycle distribution in two HCC cell lines following 24 h of treatment with DMAKN (5 μM) with or without SP600125 (20 μM). The lower panel quantified the percentage of cells in G2/M phase of the cell cycle. * $p < 0.05$, ** $p < 0.01$. (F) Cell death in HCC cells exposed to DMAKN (30 μM) with or without SP600125 (20 μM) for 24 h. ** $p < 0.01$. (G) Expression of JNK in two HCC cell lines following siRNAs-mediated knockdown. (H) Flow cytometry analyses (upper panel) illustrated the cell cycle distribution in two HCC cell lines following 24 h of treatment with DMAKN (5 μM) and JNK knockdown. The lower panel quantified the percentage of cells in the G2/M phase of the cell cycle. * $p < 0.05$, ** $p < 0.01$. (I) Cell death in two HCC cells exposed to DMAKN (30 μM) with JNK knockdown for 24 h. * $p < 0.05$, ** $p < 0.01$.

cells.

Low-dose DMAKN affects the phosphorylation status of CDK1 and CDC25C

The activity of CDK1/Cyclin B1 complex depends on the phosphorylation status of CDK1(Hartwell and Kastan, 1994). Phosphorylation at Thr-161 activates the complex, while reversible phosphorylation at Thr-14 and Tyr-15 inhibits its kinase activity (Porter and Donoghue, 2003). Therefore, we examined the impact of DMAKN on CDK1 phosphorylation in HCC cells. Results shown in Fig. 3D revealed a notable decrease in CDK1 phosphorylation at Thr-161 following DMAKN treatment in both cell lines, accompanied by increased phosphorylation at Tyr-15 and Thr-14. These findings suggest DMAKN-induced G2/M phase arrest correlates with reduced CDK1-Cyclin B1 binding due to diminished Thr-161 phosphorylation and decreased CDK1 kinase activity attributed to heightened Thr-14 and Tyr-15 phosphorylation.

Furthermore, we assessed DMAKN's influence on Cdc25C expression and phosphorylation in HCC cells. Cdc25C facilitates CDK1 dephosphorylation at Thr-14 and Tyr-15 (Peng et al., 1997; Timofeev et al., 2010). As shown in Fig. 3E, DMAKN treatment led to a significant decrease in Cdc25C expression, along with a simultaneous increase in Cdc25C phosphorylation at Ser-216. These findings underscore DMAKN's role in modulating CDK1 phosphorylation status, which is crucial for cell cycle progression. This modulation is achieved by inhibiting Cdc25C activity through upregulated Cdc25C phosphorylation at Ser-216.

DMAKN induces non-apoptotic cell death in HCC cells at high doses

Previous studies have investigated shikonin-induced apoptosis across various cancer types (Tang et al., 2016; Wang et al., 2020), leading us to hypothesize that high-dose DMAKN might similarly trigger apoptosis. To test this hypothesis, we initially employed flow cytometry with Annexin V-FITC/PI double staining, a standard method for assessing apoptosis (Gong et al., 2022). As shown in Fig. 4A, high-dose DMAKN treatment resulted in rapid $FITC^{-}/PI^{+}$ staining, which is distinct from the $FITC^{+}/PI^{+}$ and $FITC^{+}/PI^{-}$ staining patterns observed with the apoptotic inducer STS. Concurrently, Fig.4B illustrates that HCC cells treated with high doses of DMAKN and STS exhibited different morphological changes. DMAKN-treated cells showed swelling, in contrast to the shrinkage and fragmentation observed with STS. Further analysis using the apoptotic inhibitor z-VAD-fmk did not inhibit cell death induced by high-dose DMAKN (Fig. 4C). Additionally, western blotting analysis of PARP and caspase-3, key markers of apoptosis, revealed no changes in expression levels following high-dose DMAKN treatment (**Fig. S4**). These results collectively indicate that high doses of DMAKN do not induce apoptosis in HCC cells.

High-dose DMAKN-induced cell death is necrosis in HCC cells

Based on the observed cellular changes, we investigated whether DMAKN-induced cell death involved ferroptosis or necroptosis, both of which are associated with cell swelling(Chen et al., 2023). Co-incubation with Fer-1 (a ferroptosis inhibitor) or Nec-1 (a necroptosis inhibitor) did not prevent DMAKN-induced cell death (Fig. 4D and E). Additionally, western blotting analysis of ferroptosis markers (GPX4 and SLC7A11) and necroptosis markers (RIPK1 and MLKL) showed no significant changes in expression levels (Fig. S5 and **S6**), indicating that DMAKN-induced cell death does not involve ferroptosis or necroptosis.

To further investigate, we conducted live-cell analysis to monitor morphological changes in HCC cells following high-dose DMAKN treatment. As shown in Fig. 4F, DMAKN induced rapid morphological alterations, with cells initially rounding and swelling within 6 h and exhibiting pronounced swelling and detachment from the culture medium by 24 h. Given the exclusion of ferroptosis and necroptosis, and the rapid onset of morphological changes and cell death, we conclude that high-dose DMAKN-induced cell death in HCC cells is necrosis, a passive and accidental form of cell death (Darzynkiewicz et al., 1997).

ROS mediate differential effects of DMAKN: induction of cell cycle arrest at low doses and necrosis at high doses in HCC cells

ROS play a crucial role in regulating cell cycle progression and cell death (Lin et al., 2024). To investigate the anti-HCC mechanisms of DMAKN, we examined its impact on cellular ROS levels. Preliminary experiments indicated that high doses of DMAKN ($\geq$ 10 μM) rapidly elevated intercellular ROS levels, leading to swift cell death (data not shown). Consequently, we measured ROS levels after 4 h of high-dose DMAKN treatment. In contrast, low doses of DMAKN ($\leq$ 5 μM) caused a more gradual increase in ROS, with levels measured after 24 h of treatment. As illustrated in Fig. 5A, high-dose DMAKN induced a sharp rise in intracellular ROS within 4 h, whereas low-dose DMAKN led to a more gradual increase over 24 h.

To confirm the involvement of ROS in high-dose DMAKN-induced necrosis, we co-administered NAC, a ROS scavenger, with high-dose DMAKN. As shown in Fig. 5B, NAC inhibited ROS accumulation in HepG2 and Huh7 cells following high-dose DMAKN treatment. Additionally, NAC prevented necrosis in these cells, as depicted in Fig. 5C. We also evaluated NAC's effect on low-dose DMAKN-induced G2/M cell cycle arrest. Fig. 5D shows that NAC inhibited ROS accumulation in HepG2 and Huh7 cells treated with low-dose DMAKN, and Fig. 5E demonstrates that NAC prevented G2/M cell cycle arrest in these cells. These findings collectively suggest that both low-dose DMAKN-induced cell cycle arrest and high-dose DMAKN-induced necrosis are ROS-dependent. The distinct outcomes—cell cycle arrest *versus* cell death—are attributed to the rate of ROS production: high-dose DMAKN causes a rapid ROS spike leading to cell death, while low-dose DMAKN results in a slower ROS increase, leading to cell cycle arrest and impaired proliferation.

Low-dose DMAKN induces ROS/JNK-dependent cell cycle arrest, but high-dose DMAKN triggers JNK-independent ROS-driven necrosis

Since ROS induction is known to activate the JNK pathway, influencing both cell cycle arrest and cell death (Du et al., 2004), we investigated DMAKN's effect on the JNK pathway at both low and high doses. Results showed elevated levels of phosphorylated JNK in two HCC cell lines exposed to both dose levels of DMAKN (Fig. 6A and B). Notably, co-treatment with NAC effectively reversed DMAKN-induced JNK activation at both dose levels (Fig. 6C and D), indicating that ROS increases from both high and low doses of DMAKN can activate the JNK pathway.

To further assess JNK's role in DMAKN's anti-HCC efficacy, we employed SP600125, a JNK inhibitor. As shown in Fig. 6E, SP600125 prevented G2/M cell cycle arrest induced by low-dose DMAKN. However, it did not block high-dose DMAKN-induced necrosis in HCC cells (Fig. 6F). Additionally, siRNAs were used to knock down JNK expression in HCC cells (Fig. 6G). As depicted in Fig. 6H, knockdown of JNK also prevented G2/M cell cycle arrest caused by low-dose DMAKN. However, as shown in Fig. 6I, JNK knockdown was ineffective against high-dose DMAKN-induced necrosis in HCC cells. These findings suggest that while low-dose DMAKN induces ROS/JNK-dependent G2/M cell cycle arrest, high-dose DMAKN triggers ROS-mediated necrosis independently of JNK, despite the observed JNK activation.

Discussion

TCM has established itself as a mainstream complementary and alternative therapy with recognized efficacy in cancer treatment. Zicao, significant in TCM for its heat-clearing and detoxifying properties, has been used to treat various diseases, including HCC (Guo et al., 2019).

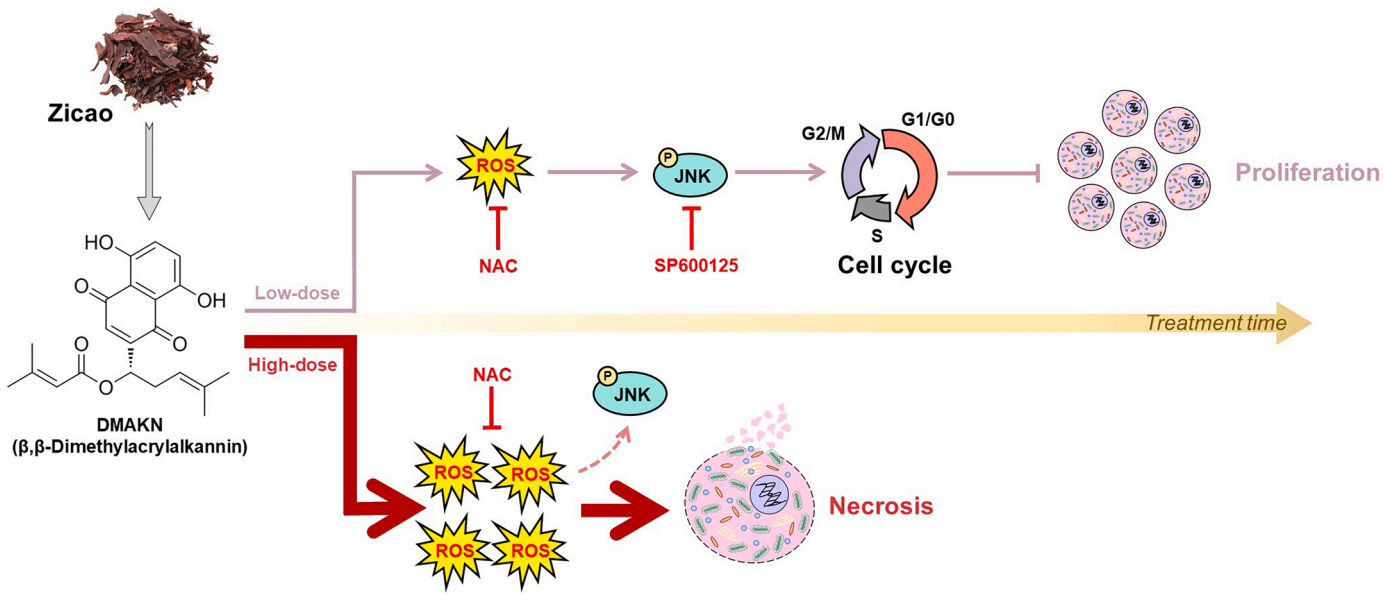

Fig. 7. Proposed mechanisms of DMAKN's anti-HCC efficacy. At high doses, DMKAN rapidly induces intracellular ROS accumulation in HCC cells, leading to necrosis. Although the JNK pathway is activated during this process, necrosis occurs independently of JNK. At low doses, DMAKN causes a gradual increase in ROS, which activates the JNK pathway, resulting in G2/M cell cycle arrest and, ultimately, inhibition of HCC cell proliferation.

Modern research has unveiled that Zicao is rich in naphthoquinone compounds, particularly shikonin, the most extensively studied active ingredient (Boulos et al., 2019; Kaur et al., 2022; Zhou et al., 2011). Despite shikonin's prominence, the Chinese Pharmacopoeia designates DMAKN as the quantitative marker for Zicao herb quality control, diverging from the conventional focus on shikonin. This choice underscores the importance of selecting quantitative markers with high content and stable properties to represent therapeutic components (Li et al., 2008). Therefore, we propose that DMAKN should be considered the primary representative of Zicao's activity, warranting further investigation into its therapeutic potential. Notably, there are few reports on the pharmacological activity of DMAKN.

Our study initially compared the contents of shikonin and DMAKN in Zicao, finding that DMAKN levels were significantly higher. This supports the Chinese Pharmacopoeia's choice of DMAKN as the quantitative marker for Zicao. Using bioinformatics methods, we identified 25 active ingredients linked to Zicao's anti-HCC activity and 15 key targets. Notably, DMAKN interacted with five targets, the highest number compared to shikonin's single target. These results suggest that DMAKN is the key component driving Zicao's anti-HCC activity, meriting further investigation into its effects and mechanisms. Subsequently, we compared the inhibitory effects on HCC cell viability between DMAKN and shikonin. Our findings demonstrated that both compounds significantly reduced the viability of HCC cells, with no difference in their activity levels. To further verify the anti-HCC activity of DMAKN, we performed a colony formation assay and constructed a xenograft nude mouse model. These experiments confirmed that DMAKN inhibited HCC cell proliferation *in vitro* and tumor growth *in vivo*.

Additionally, we focused on examining the induction of cell death by DMAKN, a hallmark of anticancer strategies (Hanahan and Weinberg, 2011). Through PI staining with flow cytometry and a 3D *in vitro* cell culture model, we discovered that DMAKN exhibited distinct abilities to induce cell death based on its dosage. Specifically, high doses of DMAKN rapidly induced significant cell death in HCC cells, whereas low doses caused minimal cell death, even over prolonged periods. Combined with the results of DMAKN's inhibitory effect on HCC cell viability, our findings indicate that high-dose DMAKN primarily induces cell death to exert its anti-HCC effects, while low-dose DMAKN inhibits HCC cell proliferation.

To understand the mechanisms behind DMAKN's differential anti-HCC effects based on dose, we conducted two separate investigations. First, we examined DMAKN's regulation of the cell cycle at low doses, which is essential for controlling cell proliferation. We found that low-dose DMAKN arrested HCC cells in the G2/M phase by suppressing CDK1 and Cyclin B1 expression, disrupting their binding, and altering CDK1 phosphorylation. DMAKN achieved this by inhibiting Cdc25C activity and increasing its phosphorylation at Ser-216. Second, we investigated the type of cell death induced by high doses of DMAKN. Through morphological observation, co-administration with various inhibitors representing different types of cell death, and analysis of cell death markers, we found that high-doses DMAKN-induced cell death was not due to apoptosis, ferroptosis, or necroptosis. The rapid onset of swelling and cell death suggested that high-dose DMAKN induces necrosis, a passive and accidental form of cell death, in HCC cells.

To further understand the mechanisms of high-dose and low-dose DMAKN, we investigated the role of ROS in these processes. High-dose DMAKN caused a sharp increase in intracellular ROS levels within a short time, while low-dose DMAKN gradually increased ROS levels over a long period. These findings suggest that low-dose DMAKN-induced G2/M cell cycle arrest is due to a gradual increase in ROS levels, while high-dose DMAKN rapidly induces necrosis through sharp intercellular ROS production. Experiments using the ROS scavenger NAC confirmed that DMAKN's differential anti-HCC effects are both ROS-dependent. NAC prevented both low-dose DMAKN-induced cell cycle arrest and high-dose DMAKN-induced necrosis, providing conclusive evidence for the role of ROS in DMAKN's effects.

Furthermore, we investigated the role of the JNK pathway in the ROS-mediated distinct effects of DMAKN, as it is a known downstream consequence of ROS induction(Shen and Liu, 2006). Low-dose DMAKN activated the JNK pathway, which was inhibited by NAC. Using the JNK inhibitor SP600125 or siRNAs to knock down JNK prevented cell cycle arrest, indicating that low-dose DMAKN-induced G2/M cell cycle arrest is ROS/JNK-dependent. In contrast, although high-dose DMAKN also activated the JNK pathway, SP600125 or siRNAs did not reverse the induced necrosis. This suggests that high-dose DMAKN rapidly induces necrosis through ROS, independent of JNK activation.

In conclusion, as summarized in Fig. 7, our study not only validates DMAKN as the main representative component of Zicao's anti-HCC activity but also underscores its significant differential effects based on dose. At low doses, DMAKN induces a gradual increase in ROS, which

activates the JNK pathway over time, leading to cell cycle arrest and inhibition of HCC cell proliferation. Thus, the low-dose DMAKN-induced arrest is ROS/JNK-dependent. Conversely, high doses rapidly overwhelm cells with ROS, directly inducing necrosis. Although JNK is activated in this process, it is JNK-independent. These dual mechanisms highlight the versatility of DMAKN as a therapeutic agent for HCC. Our findings pave the way for further exploration of DMAKN, offering a fresh perspective in the quest for effective HCC treatments.

Ethics approval and consent to participate

All animal experimental procedures were performed according to the Institutional Guidelines and Animal Ordinance of the Department of Health, and approved by the Hong Kong Polytechnic University Animal Subjects Ethics Sub-committee (21–22/176-ABCT-R-SZG, 29 May 2022).

Fundings

This research was funded by Shenzhen Science and Technology Program (JCYJ20220531090802006), Innovation and Technology Fund-Mainland-Hong Kong Joint Funding Scheme (MHP/010/20), The Hong Kong Polytechnic University Shenzhen Research Institute Life Science Research Start-up Fund (I2023A008), Chongqing Science and Technology Commission (CSTB2023NSCQ-MSX0155), and Traditional Chinese Medicine Bureau of Guangdong Province (20240410191604902O).

CRediT authorship contribution statement

Li-Sha Shen: Writing – original draft, Validation, Methodology, Investigation, Formal analysis. **Jia-Wen Chen:** Investigation, Formal analysis. **Rui-Hong Gong:** Investigation. **Zesi Lin:** Investigation. **Yu-Shan Lin:** Investigation. **Xing-Fang Qiao:** Investigation. **Qian-Mei Hu:** Investigation. **Yong Yang:** Project administration, Funding acquisition. **Sibao Chen:** Supervision, Project administration, Funding acquisition. **Guo-Qing Chen:** Writing – review & editing, Supervision, Project administration, Investigation, Funding acquisition, Conceptualization.

Declaration of competing interest

The authors declare that the research was conducted in the absence of any commercial or financial relationships that could be construed as a potential conflict of interest.

Supplementary materials

Supplementary material associated with this article can be found, in the online version, at doi:10.1016/j.phymed.2024.155959.

References

Abou-Alfa, G.K., Lau, G., Kudo, M., Chan, S.L., Kelley, R.K., Furuse, J., Sukeepaisarnjaroen, W., Kang, Y.K., Van Dao, T., De Toni, E.N., 2022. Tremelimumab plus durvalumab in unresectable hepatocellular carcinoma. NEJM. Evid. 1. EVIDoa2100070.

Boulos, J.C., Rahama, M., Hegazy, M.E.F., Efferth, T., 2019. Shikonin derivatives for cancer prevention and therapy. Cancer Lett. 459, 248–267.

Chen, J.W., Chen, S., Chen, G.Q., 2023. Recent advances in natural compounds inducing non-apoptotic cell death for anticancer drug resistance. Cancer Drug Resist. 6, 729.

Chunarkar-Patil, P., Kaleem, M., Mishra, R., Ray, S., Ahmad, A., Verma, D., Bhayye, S., Dubey, R., Singh, H.N., Kumar, S., 2024. Anticancer drug discovery based on natural products: from computational approaches to clinical studies. Biomedicines. 12, 201.

Collins, K., Jacks, T., Pavletich, N.P., 1997. The cell cycle and cancer. Proceed. Nat. Acad. Sci. 94, 2776–2778.

Darzynkiewicz, Z., Juan, G., Li, X., Gorczyca, W., Murakami, T., Traganos, F., 1997. Cytometry in cell necrobiology: analysis of apoptosis and accidental cell death (necrosis). J. Internat. Soc. Analyt. Cytol. 27, 1–20.

de Castro, T., Jochheim, L.S., Bathon, M., Welland, S., Scheiner, B., Shmanko, K., Roessler, D., Ben Khaled, N., Jeschke, M., Ludwig, J.M., 2022. Atezolizumab and bevacizumab in patients with advanced hepatocellular carcinoma with impaired liver function and prior systemic therapy: a real-world experience. Ther. Adv. Med. Oncol. 14, 17588359221080298.

Du, L., Lyle, C.S., Obey, T.B., Gaarde, W.A., Muir, J.A., Bennett, B.L., Chambers, T.C., 2004. Inhibition of cell proliferation and cell cycle progression by specific inhibition of basal JNK activity: evidence that mitotic Bcl-2 phosphorylation is JNK-independent. J. Biolog. Chem. 279, 11957–11966.

Fan, Y., Xue, H., Zheng, H., 2022. Systemic therapy for hepatocellular carcinoma: current updates and outlook. J. HepatoCell Carcinoma 233–263.

Gong, K., Li, W., 2011. Shikonin, a Chinese plant-derived naphthoquinone, induces apoptosis in hepatocellular carcinoma cells through reactive oxygen species: a potential new treatment for hepatocellular carcinoma. Free Rad. Biol. Med. 51, 2259–2271.

Gong, R.H., Chen, J.W., Shen, L.S., Lin, Y.S., Yu, H., Chen, S., Chen, G.Q., 2024. Assessing the therapeutic potential of Elephantopus scaber extract in hepatocellular carcinoma by inhibiting the PI3K/Akt pathway. J. Funct. Foods. 113, 106009.

Gong, R.H., Yang, D.J., Kwan, H.Y., Lyu, A.P., Chen, G.Q., Bian, Z.X., 2022. Cell death mechanisms induced by synergistic effects of halofuginone and artemisinin in colorectal cancer cells. Int. J. Med. Sci. 19, 175.

Guo, C., He, J., Song, X., Tan, L., Wang, M., Jiang, P., Li, Y., Cao, Z., Peng, C., 2019. Pharmacological properties and derivatives of shikonin—A review in recent years. Pharmacol. Res. 149, 104463.

Hanahan, D., Weinberg, R.A., 2011. Hallmarks of cancer: the next generation. Cell 144, 646–674.

Hartwell, L.H., Kastan, M.B., 1994. Cell cycle control and cancer. Science 266, 1821–1828.

Kaur, K., Sharma, R., Singh, A., Attri, S., Arora, S., Kaur, S., Bedi, N., 2022. Pharmacological and analytical aspects of alkannin/shikonin and their derivatives: an update from 2008 to 2022. Chin. Herb. Med. 14, 511–527.

Li, H., Wei, W., Xu, H., 2022. Drug discovery is an eternal challenge for the biomedical sciences. Acta Mater. Med. 1, 1–3.

Li, S., Han, Q., Qiao, C., Song, J., Lung Cheng, C., Xu, H., 2008. Chemical markers for the quality control of herbal medicines: an overview. Chin. Med. 3, 1–16.

Lin, Y.S., Sun, Z., Shen, L.S., Gong, R.H., Chen, J.W., Xu, Y., Yu, H., Chen, S., Chen, G.Q., 2024. Arnicolide D induces endoplasmic reticulum stress-mediated oncosis via ATF4 and CHOP in hepatocellular carcinoma cells. Cell Death. Discov. 10, 134.

Mou, L., Tian, X., Zhou, B., Zhan, Y., Chen, J., Lu, Y., Deng, J., Deng, Y., Wu, Z., Li, Q., 2021. Improving outcomes of tyrosine kinase inhibitors in hepatocellular carcinoma: new data and ongoing trials. Front. Oncol. 11, 752725.

Nath, S., Devi, G.R., 2016. Three-dimensional culture systems in cancer research: focus on tumor spheroid model. Pharmacol. Ther. 163, 94–108.

Peng, C.Y., Graves, P.R., Thoma, R.S., Wu, Z., Shaw, A.S., Piwnica-Worms, H., 1997. Mitotic and G2 checkpoint control: regulation of 14-3-3 protein binding by phosphorylation of Cdc25C on serine-216. Science 277, 1501–1505.

Porter, L.A., Donoghue, D.J., 2003. Cyclin B1 and CDK1: nuclear localization and upstream regulators. Prog. Cell Cycle Res. 5, 335–348.

Sha, F., Zhang, J., Yang, H., Hu, Y., Wei, W., Wang, C., Li, X., Shen, X., An, Y., Li, J., 2024. Systematical targeted multicomponent characterization and comparison of Arnebiae Radix and its three confusing species by offline two-dimensional liquid chromatography/LTQ-Orbitrap mass spectrometry. Anal. Bioanal. Chem. 416, 583–595.

Shen, H.M., Liu, Z.g., 2006. JNK signaling pathway is a key modulator in cell death mediated by reactive oxygen and nitrogen species. Free Rad. Biol. Med. 40, 928–939.

SHI, G., REN, Z., JIANG, Y., LU, P., 2018. Study on the quality control of Zicao ointment. Internat. J. Tradit. Chin. Med. 738–741.

Sleeman, K.E., de Brito, M., Etkind, S., Nkhoma, K., Guo, P., Higginson, I.J., Gomes, B., Harding, R., 2019. The escalating global burden of serious health-related suffering: projections to 2060 by world regions, age groups, and health conditions. Lancet Glob. Health 7, e883–e892.

Sung, H., Ferlay, J., Siegel, R.L., Laversanne, M., Soerjomataram, I., Jemal, A., Bray, F., 2021. Global cancer statistics 2020: GLOBOCAN estimates of incidence and mortality worldwide for 36 Cancers in 185 Countries. CA Cancer J. Clin. 71, 209–249.

Tang, X., Zhang, C., Wei, J., Fang, Y., Zhao, R., Yu, J., 2016. Apoptosis is induced by shikonin through the mitochondrial signaling pathway. Mol. Med. Rep. 13, 3668–3674.

Timofeev, O., Cizmecioglu, O., Settele, F., Kempf, T., Hoffmann, I., 2010. Cdc25 phosphatases are required for timely assembly of CDK1-cyclin B at the G2/M transition. J. Biolog. Chem. 285, 16978–16990.

Wang, F., Mayca Pozo, F., Tian, D., Geng, X., Yao, X., Zhang, Y., Tang, J., 2020. Shikonin inhibits cancer through P21 upregulation and apoptosis induction. Front. Pharmacol. 11, 861.

Wei, P.L., Tu, C.C., Chen, C.H., Ho, Y.S., Wu, C.T., Su, H.Y., Chen, W.Y., Liu, J.J., Chang, Y.J., 2013. Shikonin suppresses the migratory ability of hepatocellular carcinoma cells. J. Agric. Food Chem. 61, 8191–8197.

Yan, Z., Lai, Z., Lin, J., 2017. Anticancer properties of traditional Chinese medicine. Comb. Chem. High Throughput Screen. 20, 423–429.

Yuan, H., Ma, Q., Ye, L., Piao, G., 2016. The traditional medicine and modern medicine from natural products. Molecules. 21, 559.

Zhou, W., Jiang Hda, G., Peng, Y., Li, S.S., 2011. Comparative study on enantiomeric excess of main akannin/shikonin derivatives isolated from the roots of three endemic Boraginaceae plants in China. Biomed. Chromatogr. 25, 1067–1075.